Effects of Thermal Boundary Conditions During Finite Element Modeling of Physical Vapor Transport

Wade Luhman
Minnesota State University, Mankato

Effects of Boundary Conditions during
Finite Element Modeling of Physical Vapor Transport

Student Researcher: Wade Luhman, Mechanical Engineering

Faculty Advisor: Patrick Tebbe, Mechanical Engineering Department Faculty

Abstract

Physical vapor transport (PVT) is a material processing method commonly used to produce different types of semiconductor materials. Computer modeling of PVT is important to understand the fundamentals of the processing method. Due to the large amount of computer processing power and storage needed to solve the computer models many of the previously solved simulations have been simplified to efficiently utilize computer usage. Previous PVT computer simulations of mercurous chloride (Hg_2Cl_2) have assumed constant temperature profiles on the source and crystal substrate for simplicity. These simulations were performed using the FIDAP computational fluid dynamics software package. In this research the system boundary conditions for the previously solved mercurous chloride models were modified using the FIDAP software package to more accurately represent an actual PVT system. The results were then compared to the previously solved simplified cases and the boundary condition effects were examined. Previous research found that there are ranges of Rayleigh number values that give different flow structure forms. It was found that the new simulations show that the bifurcation points for the flow fields have moved to slightly higher Rayleigh number values. It was also found that some of the flows that were previously found to be in oscillation no longer oscillate with the new boundary conditions. These results are important for the crystal growth and semiconductor community in improving future processes and product quality.

Introduction

A commonly used method for crystal growth and other types of film deposition is Physical Vapor Transport (PVT). PVT is a process where a source material is heated, normally by an electrical current, and then sublimes from a solid into a vapor. The vapor is then transported through an inert gas that is backfilled into the sealed enclosure. The transport takes place largely by natural convection. The vaporized source material condenses on a cooler substrate surface. This process is depicted in Figure 1. PVT is a growth method that is especially important for crystalline semiconductor materials such as mercurous chloride that are difficult or impossible to fabricate by other deposition methods.
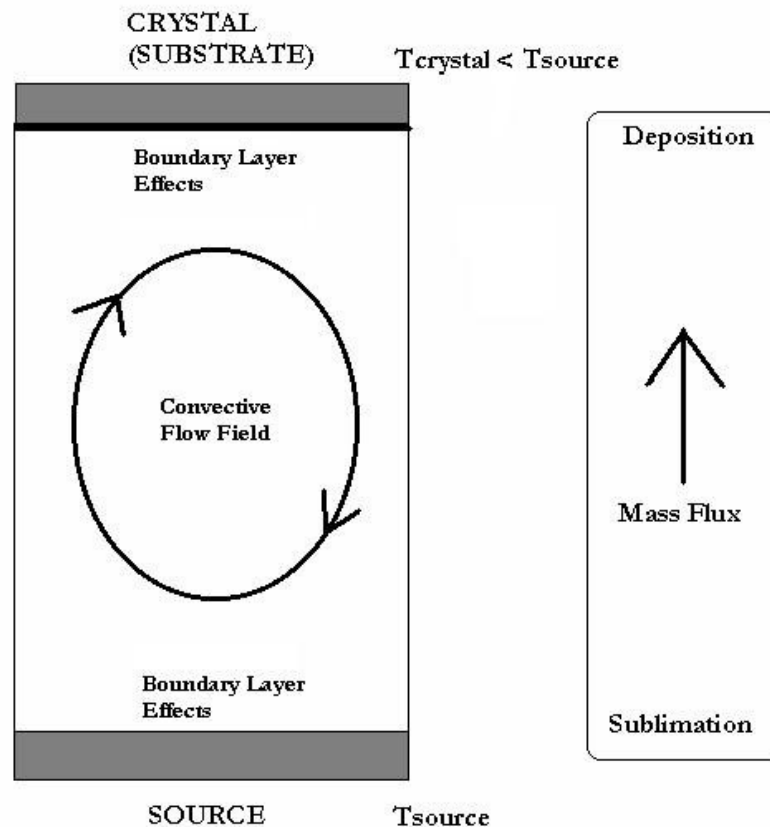
Figure 1: Schematic of a vertically oriented PVT system [1]

Previous computational work done by Duval [2] has shown that different flowfield patterns are generated by varying the Rayleigh number. The Rayleigh number is a non-dimensional number that relates the temperature difference with the inertial and natural convection in the system. Figure 2 shows the bifurcation diagram for different ranges of the Rayleigh number. This figure depicts how the flow transitions from stable to unstable oscillation. This work done by Duval was performed using a computational method to examine the flow structures. Tebbe et al. have verified in their work [1] that the FIDAP computational method will produce the same results. Their work took a number of cases that were run by Duval [2] and verified that FIDAP was able to produce credible results for transient flow analysis.
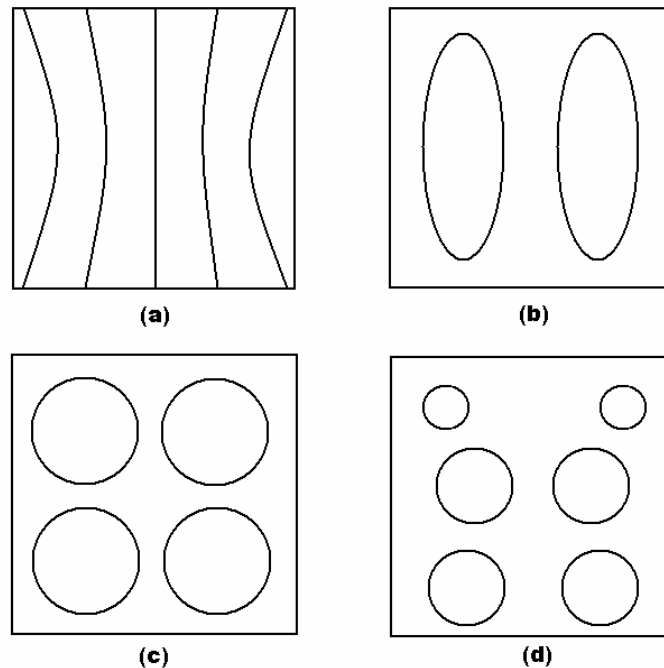
Figure 2: Bifurcation diagram for different ranges of Raleigh number [1]
(a) $0 < Ra_T < 9.0 \times 10^3$ Stable
(b) $9.0 \times 10^3 < Ra_T < 8.0 \times 10^4$ 2 cells
(c) $8.0 \times 10^4 < Ra_T < 7.0 \times 10^5$ 4 cells, stable oscillation
(d) $7.0 \times 10^5 < Ra_T < 4.05 \times 10^6$ 6 cells, unstable oscillation

Method of Research

The objective of this research was to extend the work done by Tebbe et al.. For this research we looked at running computational simulations that more accurately represent an actual system. In previous research the crystal was extended over the entire width of the enclosure. To create a system that more closely represents an actual PVT module the crystal size was reduced to 20% of the enclosure width (Figure 3). Four different cases from previous research were selected to run with the new smaller crystal size. The parameters for each case are displayed in Table 1. To compare the different situations the streamline contour plots for each will be compared. The bifurcation points and flow patterns will also be examined. A bifurcation point occurs when the flow transitions from one form to another. Time history plots for the x and y component velocities at similar points in the system will also be compared in order to look at the effects the boundary conditions have on the flowfields.
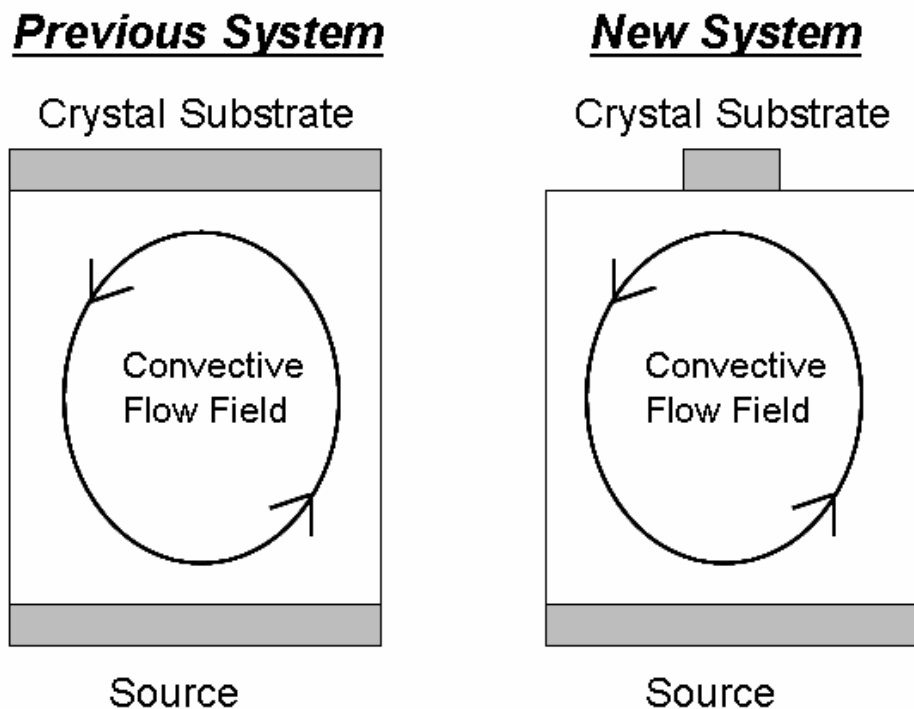
Figure 3: Schematics of previous and current PVT systems

Table 1: Parameters for PVT cases

Case	Ra_T	Ra_s	Pr	Le	Pe	C_v	⊗T	⊗t*
1	3.83×10^4	0	0.871	0.411	0.876	1.71	2	0.00125
2	1.80×10^5	0	0.831	0.366	1.90	1.28	7.5	0.00125
3	8.19×10^5	0	0.758	0.5	2.96	1.06	20	0.000125
4	1.92×10^6	0	0.717	0.54	3.50	1.03	30	0.000125

Results and Comparison

The streamline contour plots for each case were examined over the length of the simulation. The cases were carried out using the same dimensionless time constant, t*, that was used in previous research [1]. In doing this the bifurcation points could be determined and the cases could be compared to previous research. Each of the four simulated cases will be looked at individually.

Case 1

Case 1 showed very similar results to that of previous research. Previous research stated that the initial parabolic flowfield would transition into a two-cell pattern [1]. This research shows that the streamlines for this case slowly progressed from initial conditions, shown in Figure 4, to a two-cell structured flow. The two-cell flow field stabilized at t* = 0.0563 and remained in that form for the remaining length of the simulation. Figure 5 shows the streamlines at t* = 1.00 which is the last time step of the simulation for this case. The x and y component velocity time history plots for Case 1 are shown in Figures 6 and 7 respectively. Both figures show that the velocity stabilizes between t* values of 0.20 and 0.40 and remains there throughout the duration of the simulation.
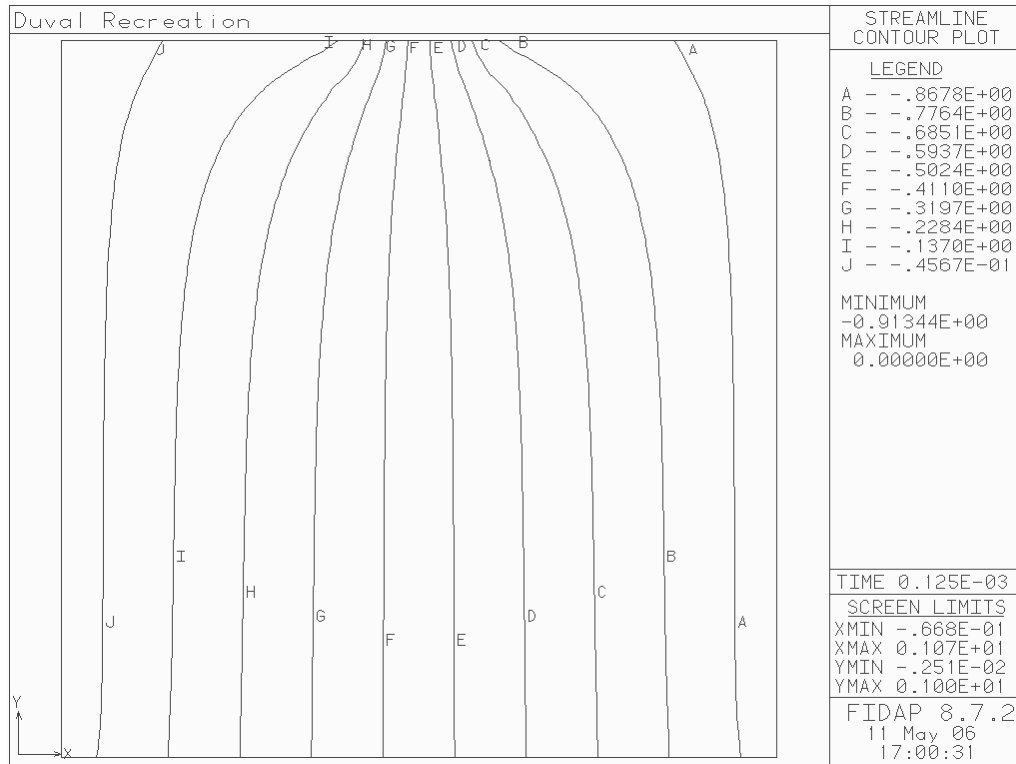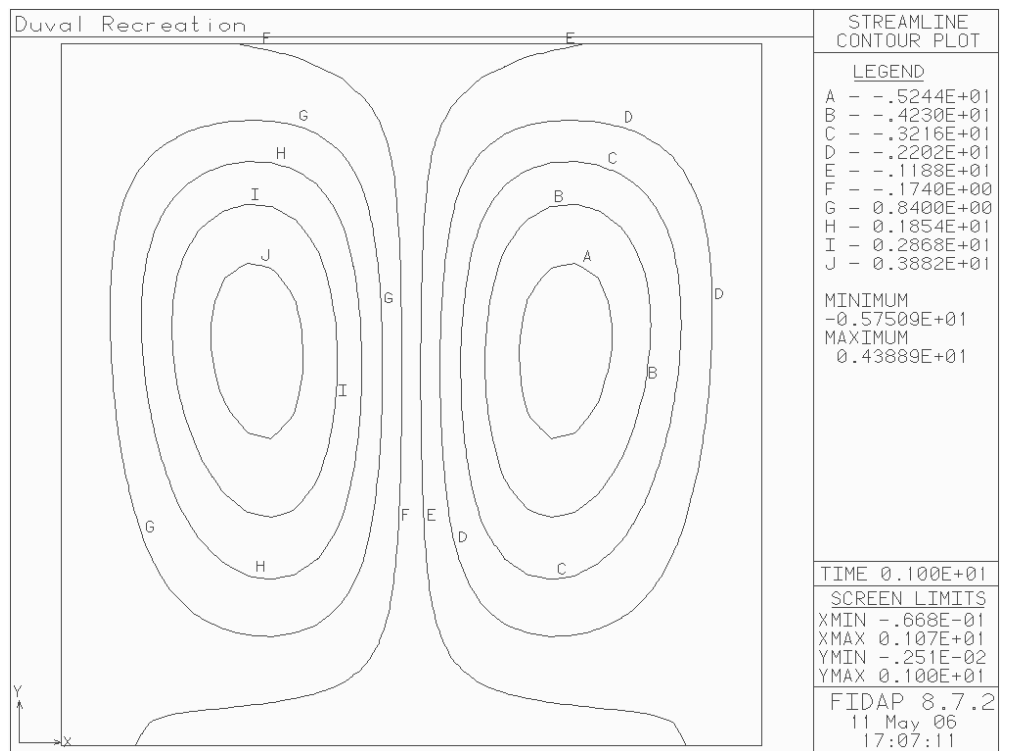
Figure 4: Flow structure for Case 1 at t* = 0.000125

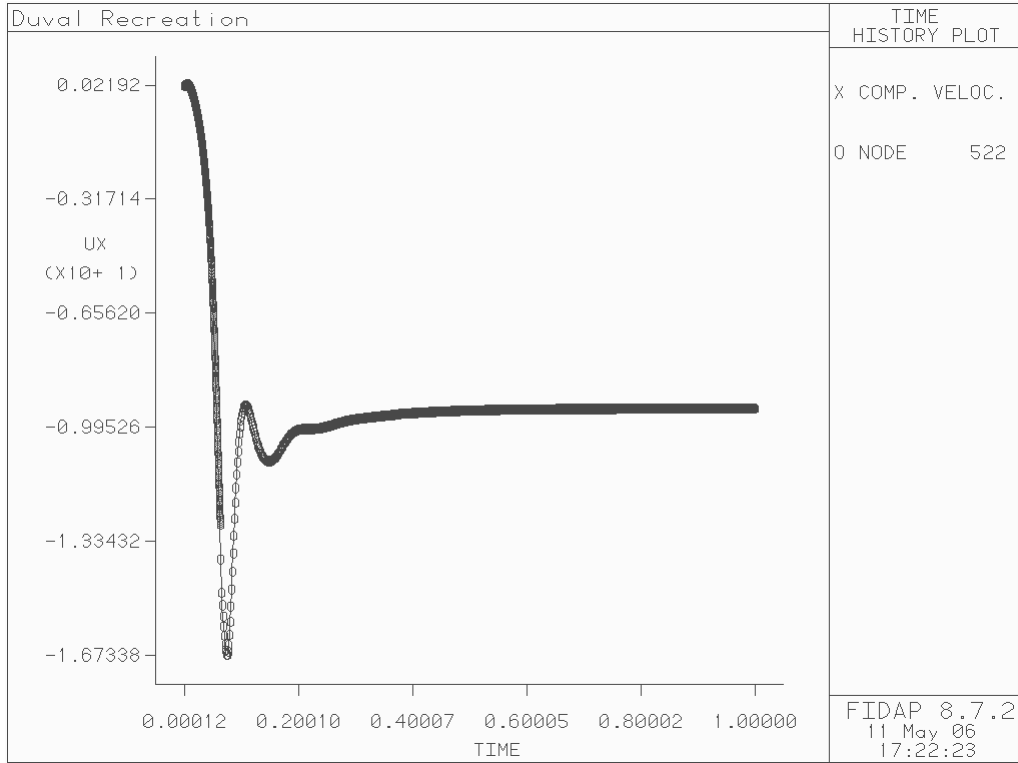Figure 5: Flow structure for Case 1 at t* = 1.00

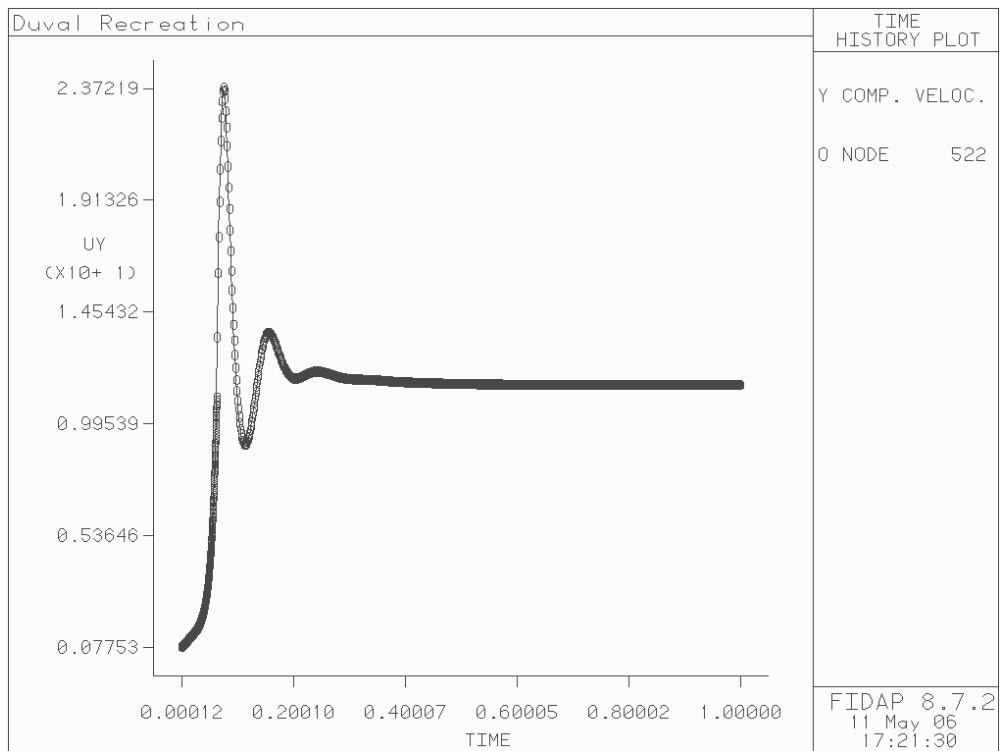Figure 6: Case 1 x-component velocity at a fixed point (0.333, 0.7)

Figure 7: Case 1 y-component velocity at a fixed point (0.333, 0.7)

Case 2

For Case 2 the previously run cases showed that the flowfield developed into an two-cell structure, transitioned into a four-cell structure and stabilized with a unicellular flow pattern. The new cases with the smaller crystal size start similarly with a two-cell structure but stay in that structure and stabilize. The two-cell structure is initially formed at $t^* = 0.025$. The case was run out for a longer length of time to see if the other flow patterns previously found would develop. The case was run until $t^* = 2.00$ and no transitions were found. The flow structure can be seen in Figure 8. Since the case was stable for such a large amount of time it is reasonable to assume that the previously seen transitions were not going to occur. This shows a difference between the previously run case and the current one. When looking at the time history plots for the x and y component velocities, Figures 9 and 10, both figures show the same trend. The x and y direction velocities stabilize and the flowfields do not oscillate over time. The point selected to display the x and y component velocities is the same as that in previous research. In doing this the current simulation could be compared to the previous results. Both cases show that the velocity stabilizes over time.
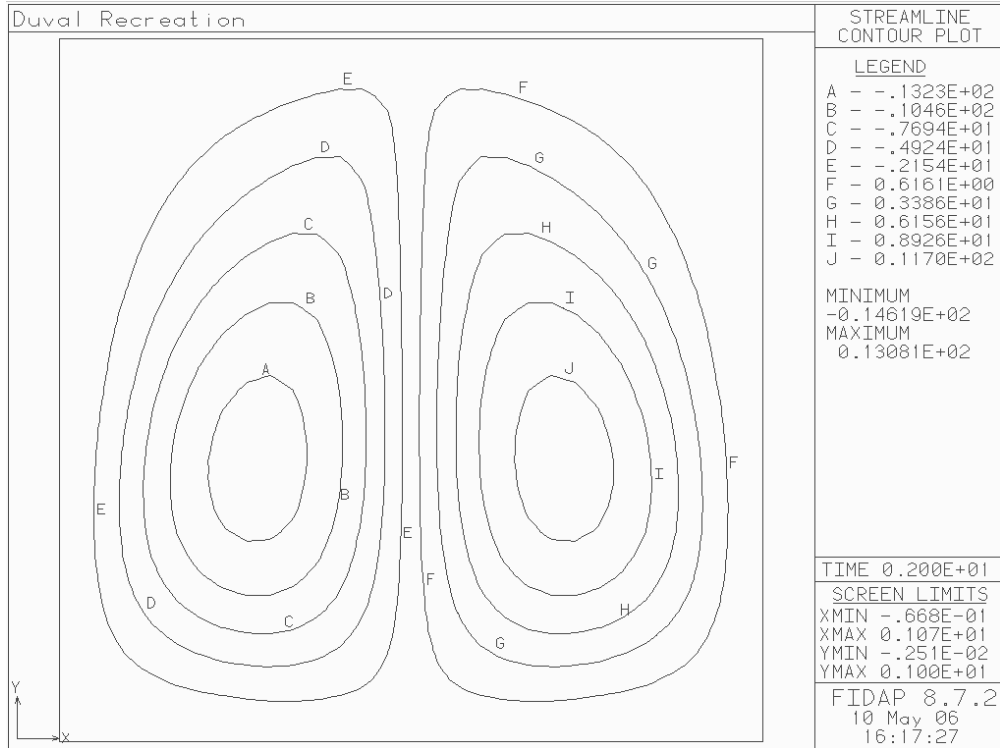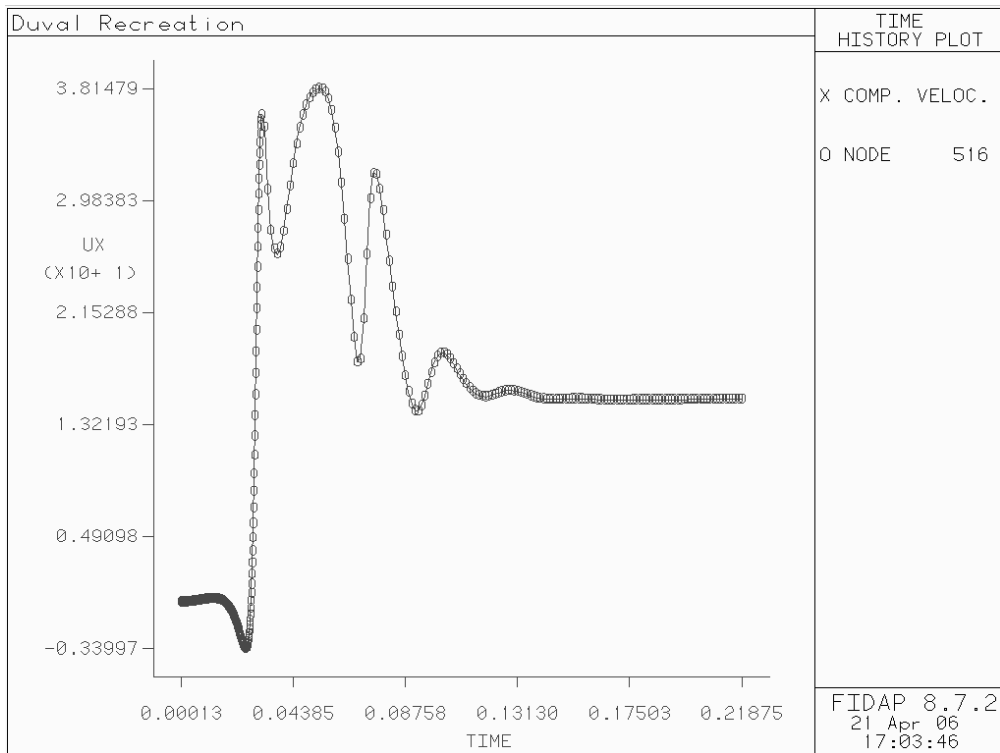
Figure 8: Flow structure for Case 2 at t* = 2.00

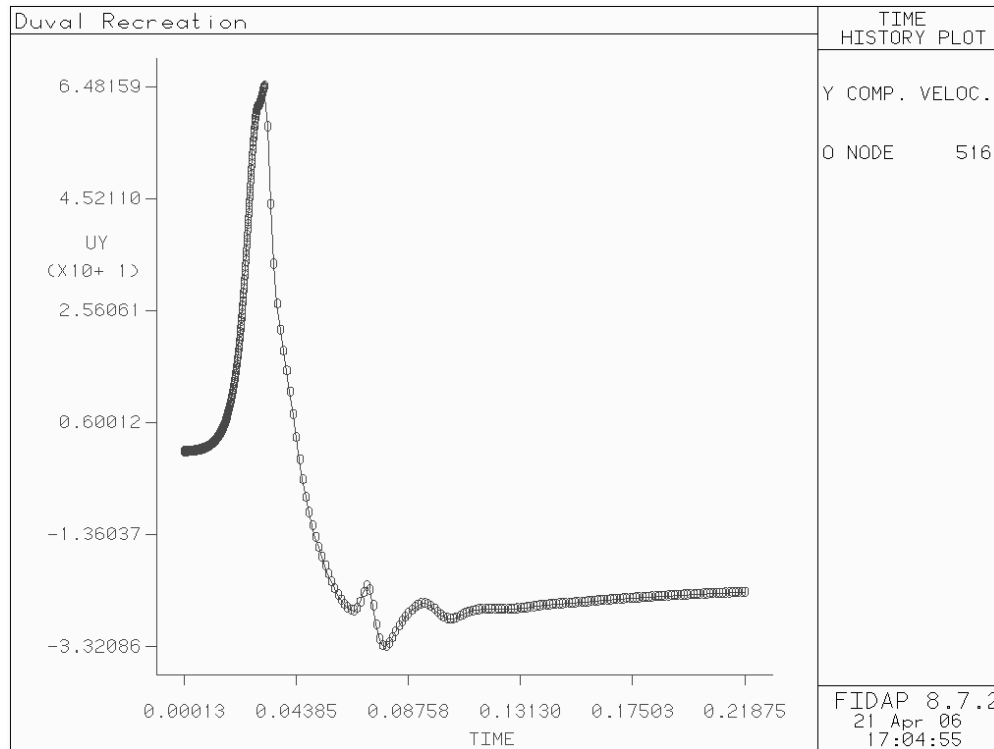Figure 9: Case 2 x-component velocity at a fixed point (0.33, 0.5)

Figure 10: Case 2 y-component velocity at a fixed point (0.33, 0.5)

Case 3

When looking at the streamline plots for Case 3 some new and interesting developments were found. The previous results for this case showed that the streamlines progressed as they did for Case 2 in previous research; however, after the four-cell structure develops the flowfield becomes unstable before transitioning into a unicellular structure. The new simulation shows the same transitions until the end when the flowfields stabilize into a two-cell structure instead of a one-cell structure. The flowfields for both the previous and current cases develop at close to the same times at the beginning. The transition from the four-cell structure to an unstable flow for the current simulation occurs at a slightly later time of t* = 0.106 than the t* = 0.066 for the previously run case. The two-cell flow initially forms at t* = 0.119 and then stays in a two-cell form but does not stabilize until t* = 0.212. Over this time period the two cells fluctuate in size and position until fully

stabilizing. The case was carried out to t* = 0.594 and the flowfield remained stable. The development of the flowfields is depicted in Figures 11 - 15. Another large difference between the previous and newly run cases shows up in the time history velocity plots. The time history plots for the previous simulations show that over time the velocity continues to oscillate. For the current simulation with the smaller crystal size the time history plot shows that the velocity is converging to a steady state value. This is important for the product quality as the crystal is growing. Without the oscillations the crystal will form more uniformly with fewer imperfections. The time history plots for the previous research are shown in Figures 16 and 17 where as the plots for this research are shown in Figures 18 and 19.
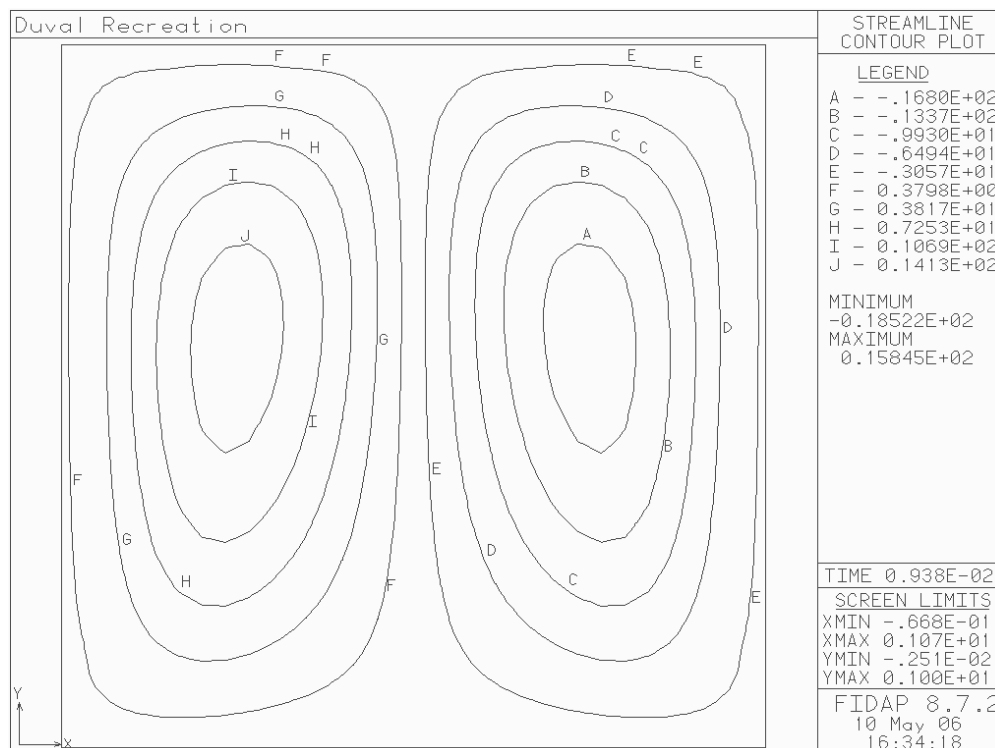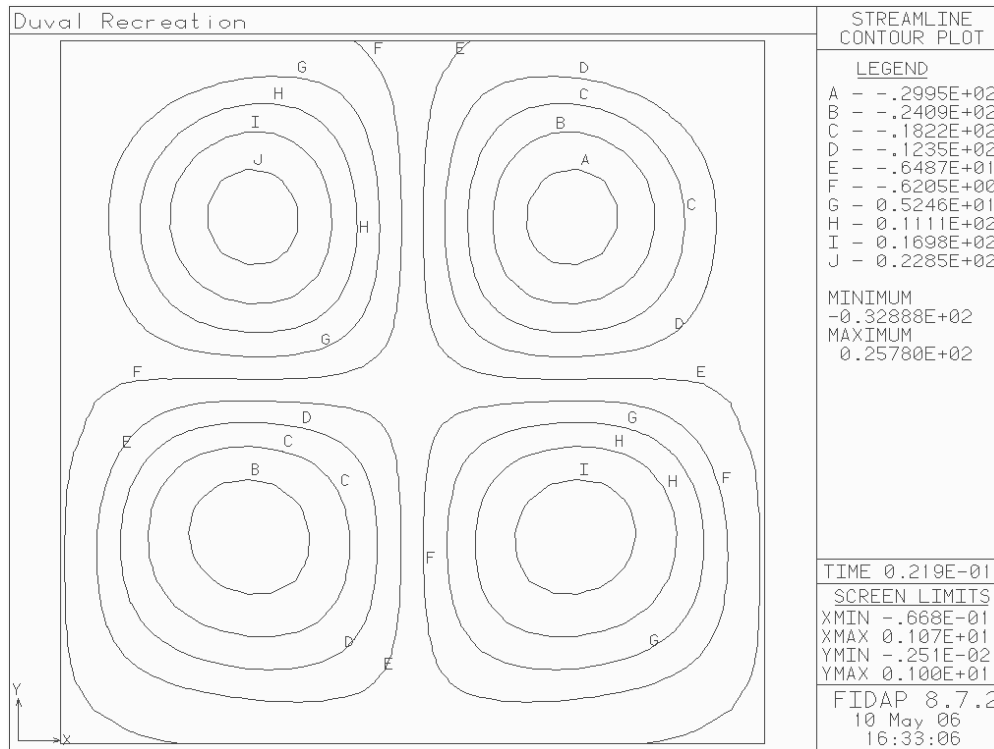

Figure 11: Flow structure for Case 3 at t* = 0.00938
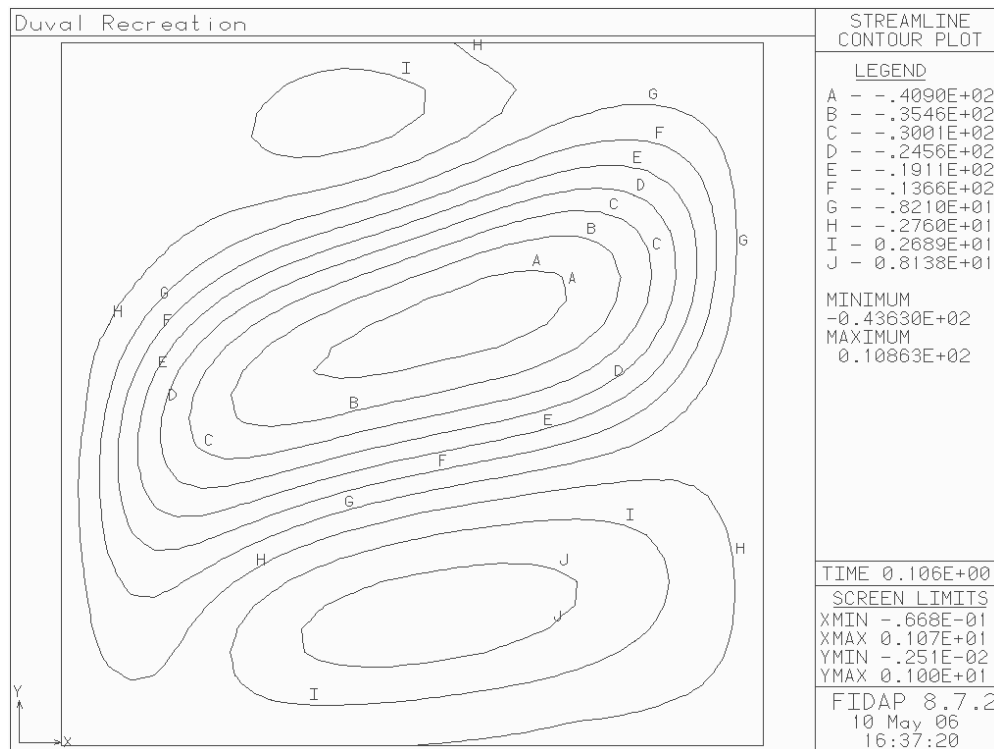
Figure 12: Flow structure for Case 3 at t* = 0.0219
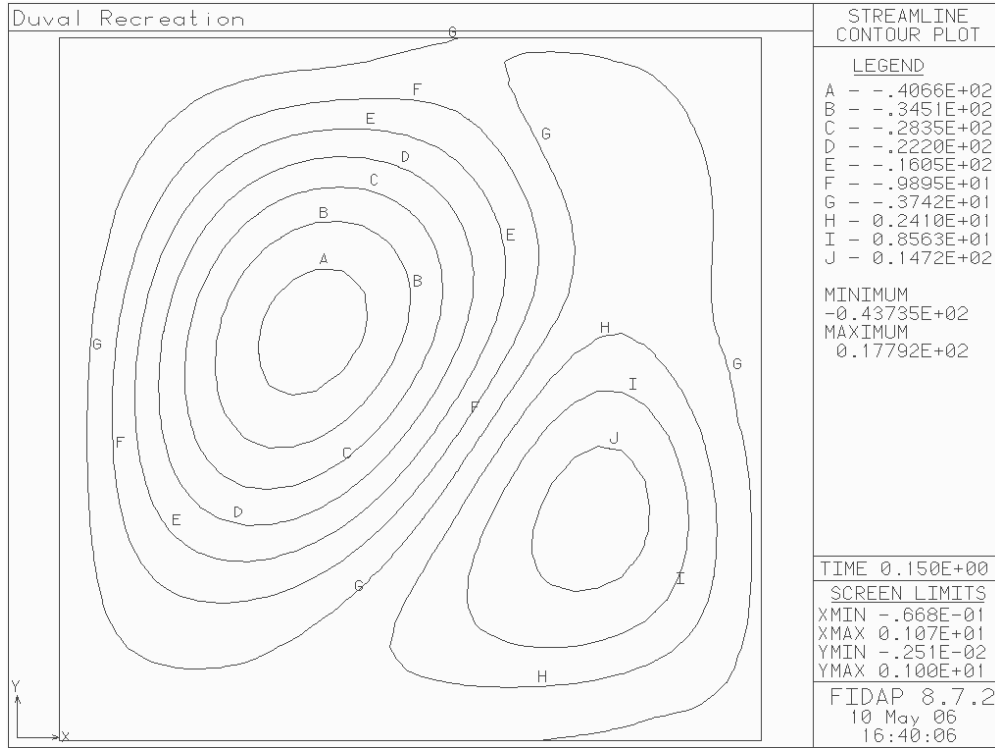

Figure 13: Flow structure for Case 3 at t* = 0.106
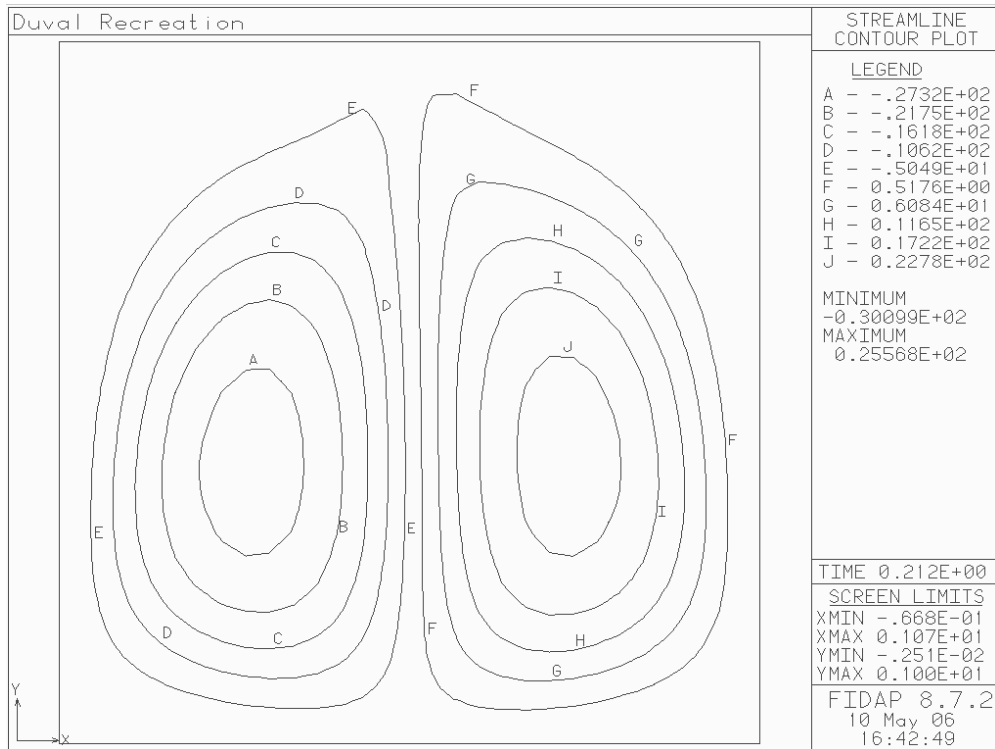
Figure 14: Flow structure for Case 3 at t* = 0.150

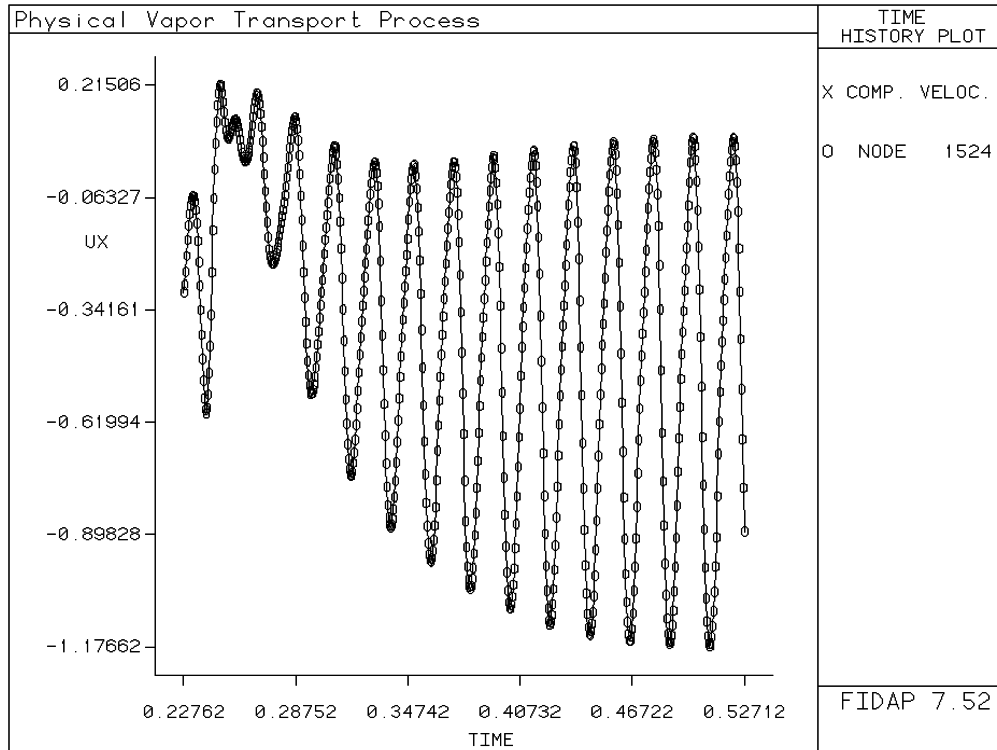Figure 15: Flow structure for Case 3 at t* = 0.212

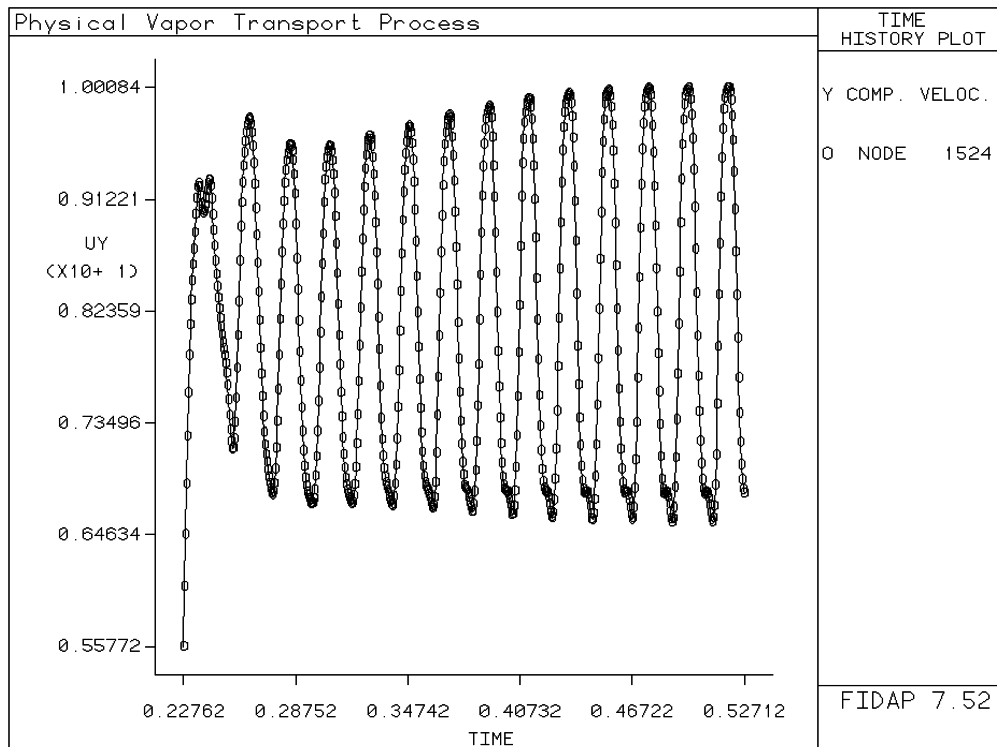Figure 16: Previous Case 3 x-component velocity at a fixed point (0.98, 0.4) [1]

Figure 17: Previous Case 3 y-component velocity at a fixed point (0.98, 0.4) [1]
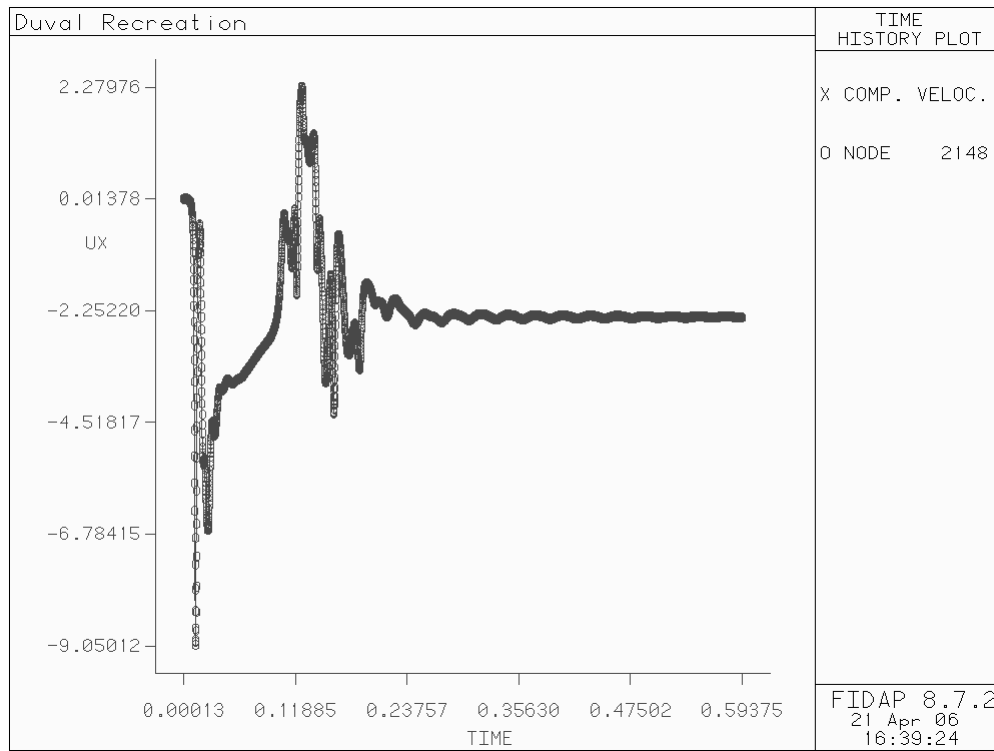
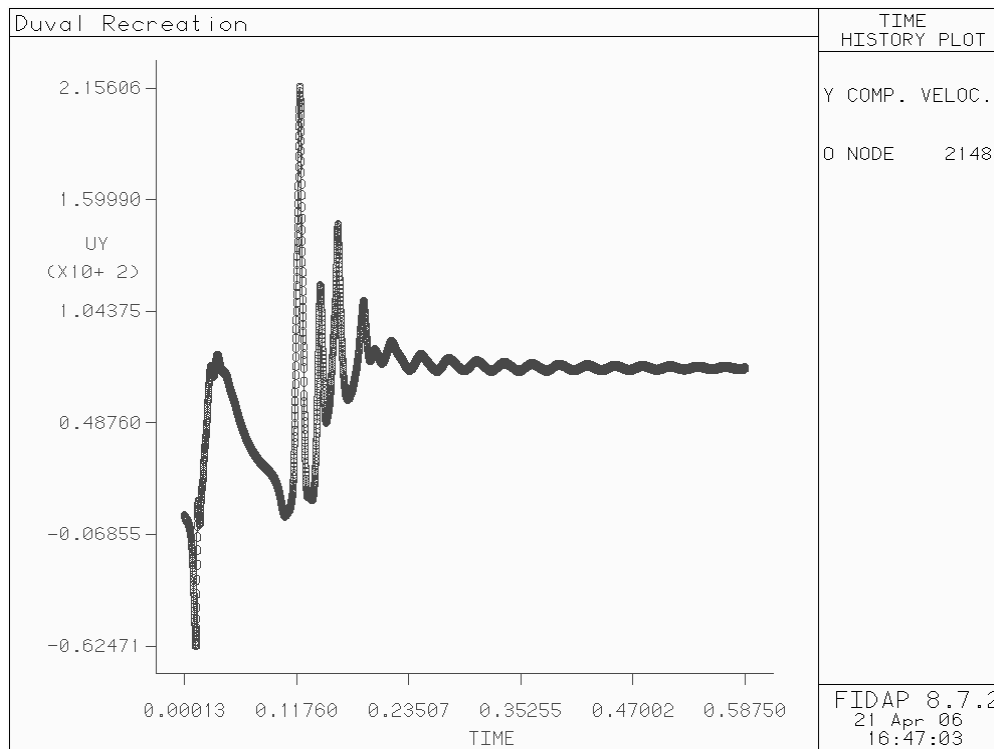Figure 18: New Case 3 x-component velocity at a fixed point (0.98, 0.4)

Figure 19: New Case 3 y-component velocity at a fixed point (0.98, 0.4)

Case 4

Case 4 has the largest Rayleigh number value of the four cases and shows more erratic flow transitions than the previous three cases. The flowfield quickly develops into a two-cell structure at t* = 0.000313. After this field is formed two smaller circulation cells develop inside each of the larger cells. The flowfield then transitions into a two-cell structure without the smaller circulation cells as it did cases 1, 2 and 3 but quickly formed into a four-cell flowfield and two different variations of six-celled structures after that. The last six-cell structure is seen at t* = 0.00356. For a period of time until t* = 0.0216 the flowfield is very unstable and forms a number of different flow structures having anywhere from two to five different convection cells. After this transition period a large unicellular flow structure is formed. This one-cell flowfield continues throughout the remaining length of the simulation. The simulation was run until t* = 0.102. During the latter part of the simulation, with the unicellular flowfield, there continues to be smaller convection cells that form in the corners of the enclosure that slightly move the much larger one-cell flowfield. Over time the smaller cells varied randomly in number anywhere from one to three different cells over the length of the simulation. Figures 20 through 31 show the evolution of the flowfield for this case. The time history plots again show the x and y component velocities. The figures show that the velocities are stabilizing. However, they are slightly more erratic than the previous cases.
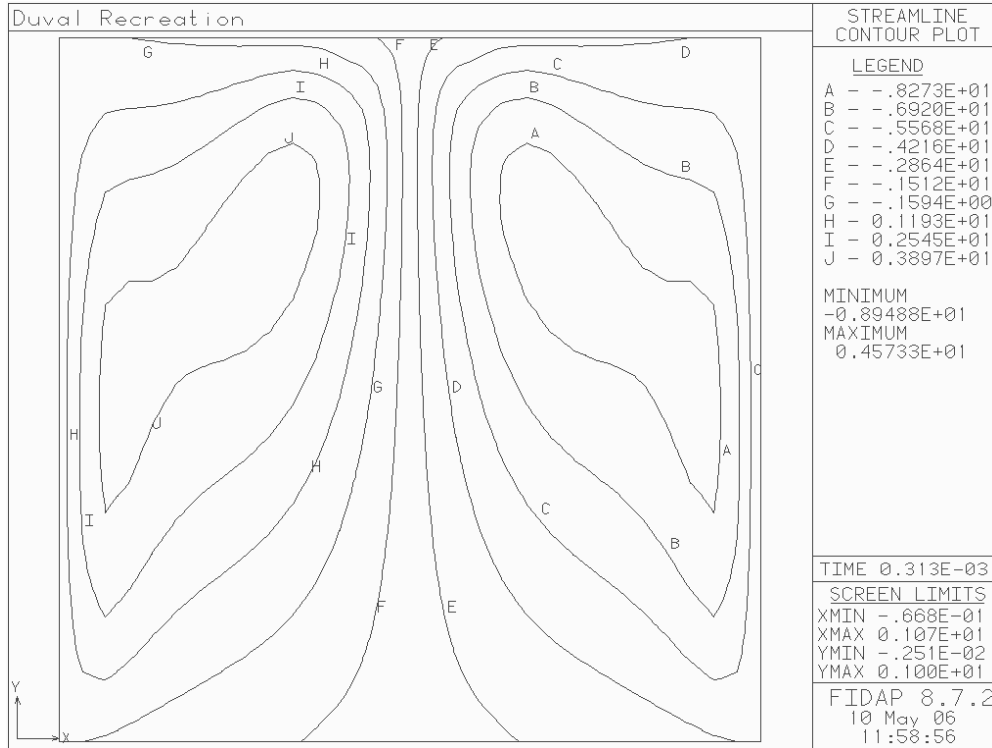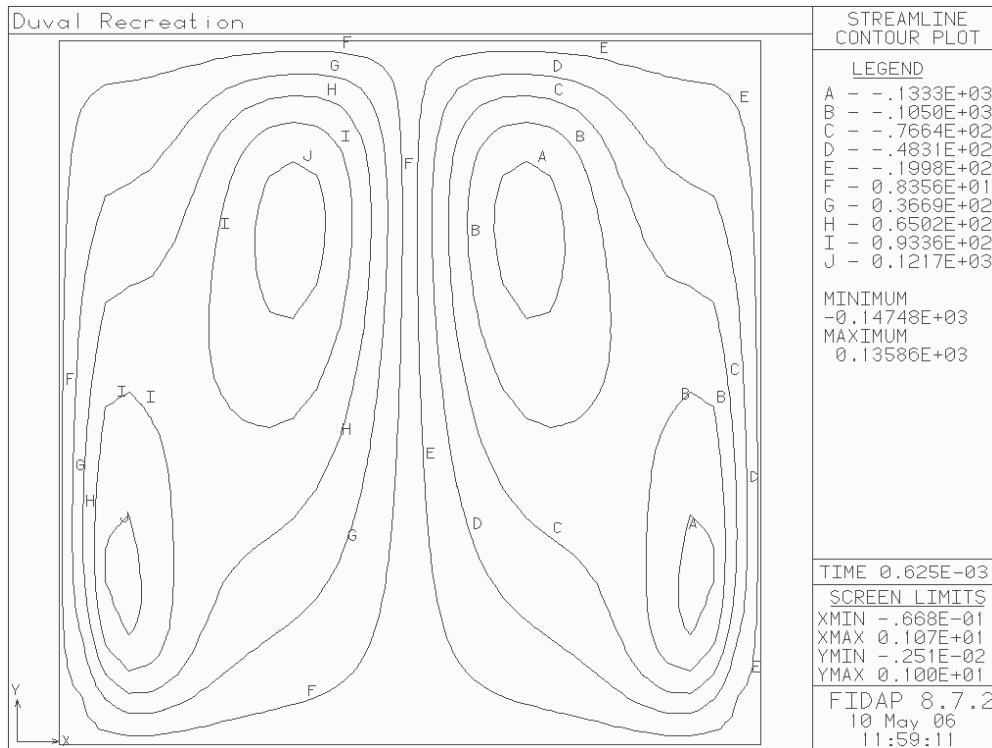
Figure 20: Flow structure for Case 4 at t* = 0.000313
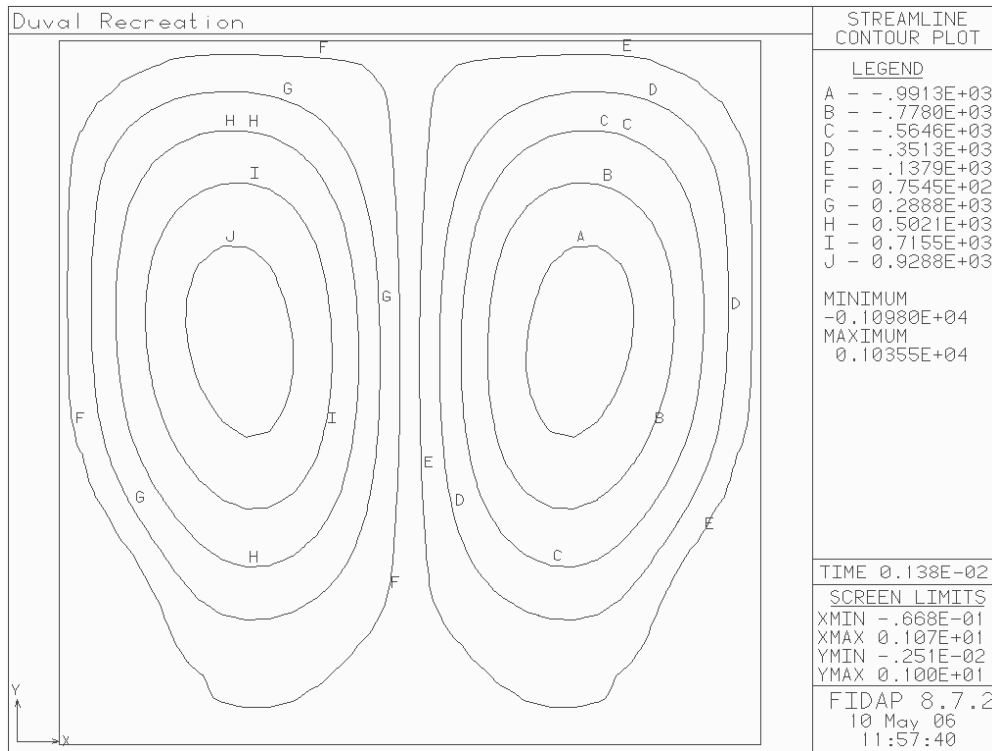

Figure 21: Flow structure for Case 4 at t* = 0.000625

Figure 22: Flow structure for Case 4 at t* = 0.00138
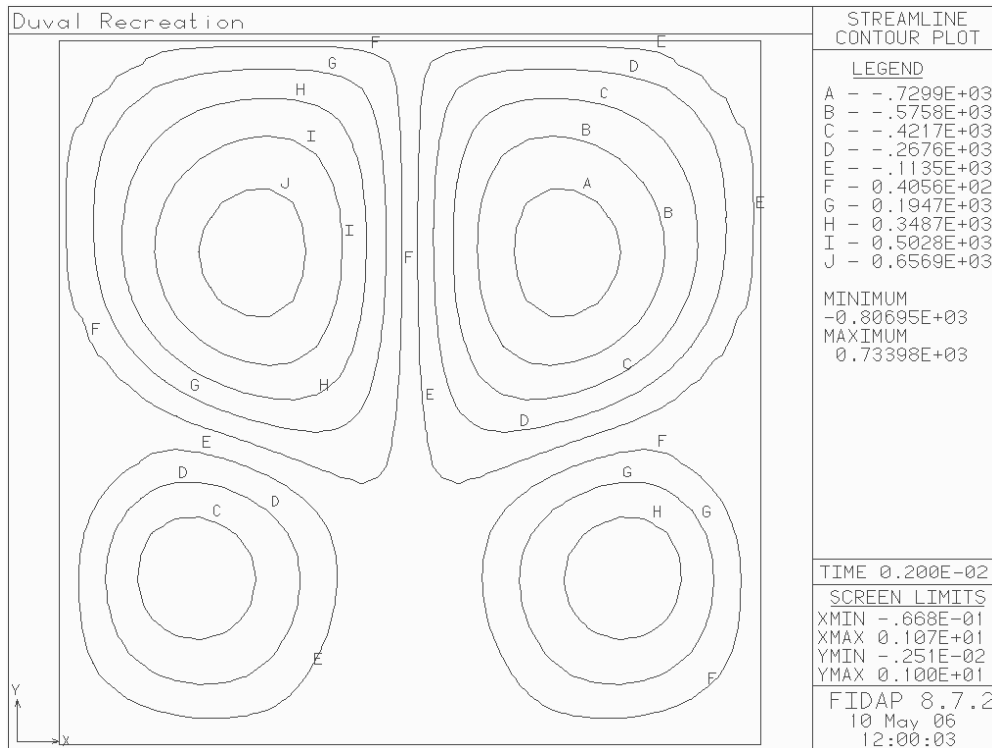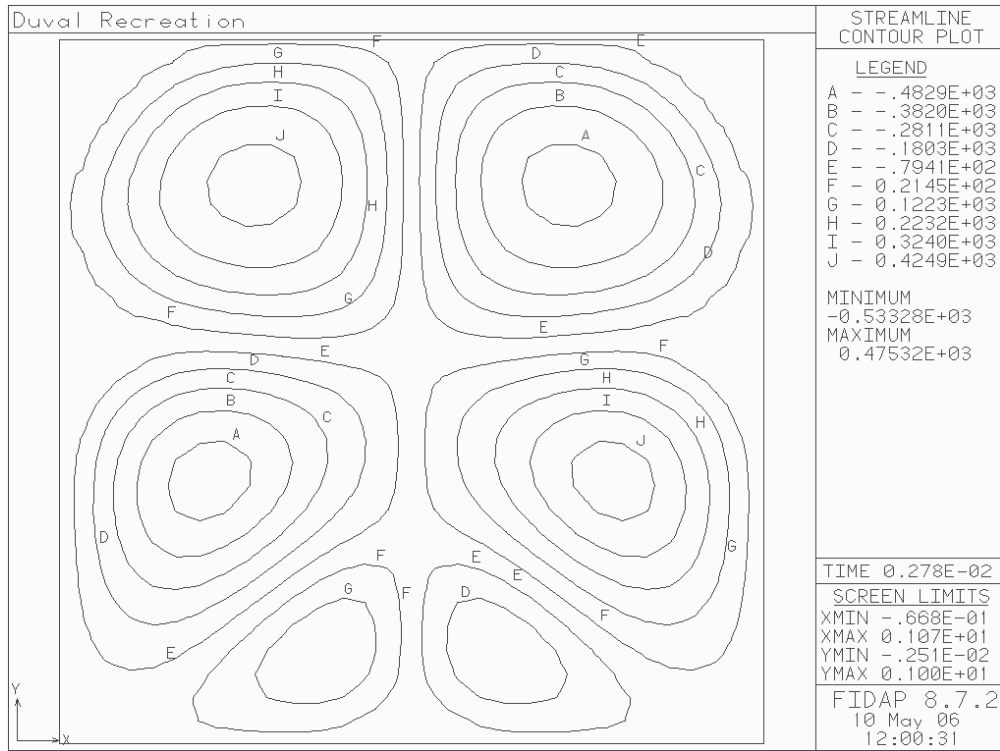

Figure 23: Flow structure for Case 4 at t* = 0.0020
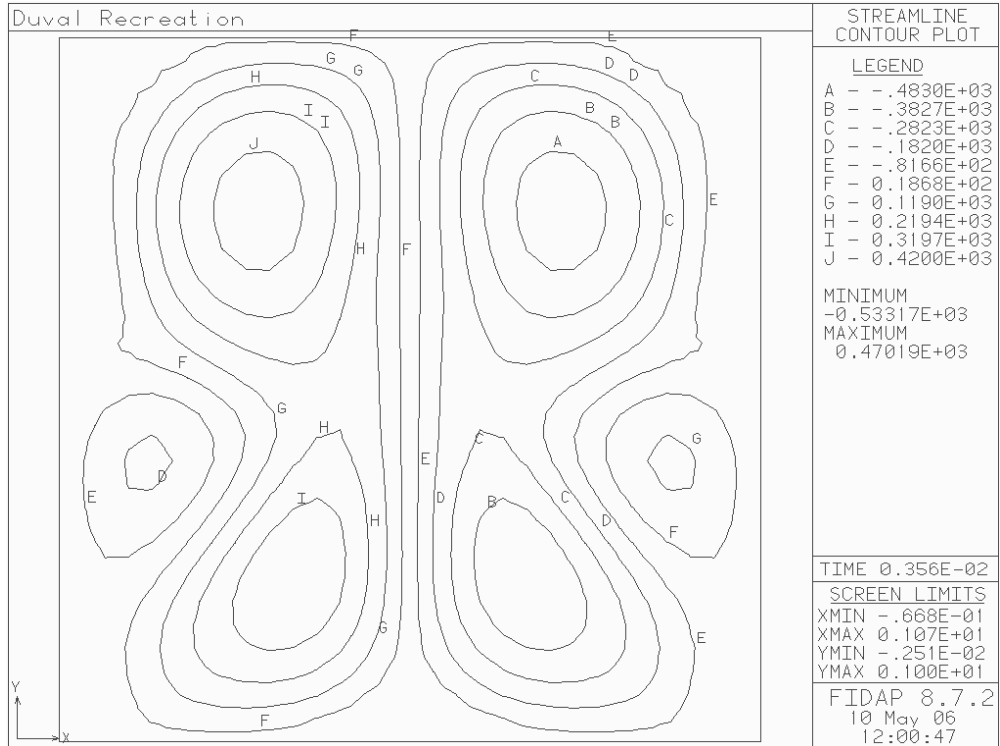
Figure 24: Flow structure for Case 4 at t* = 0.00278
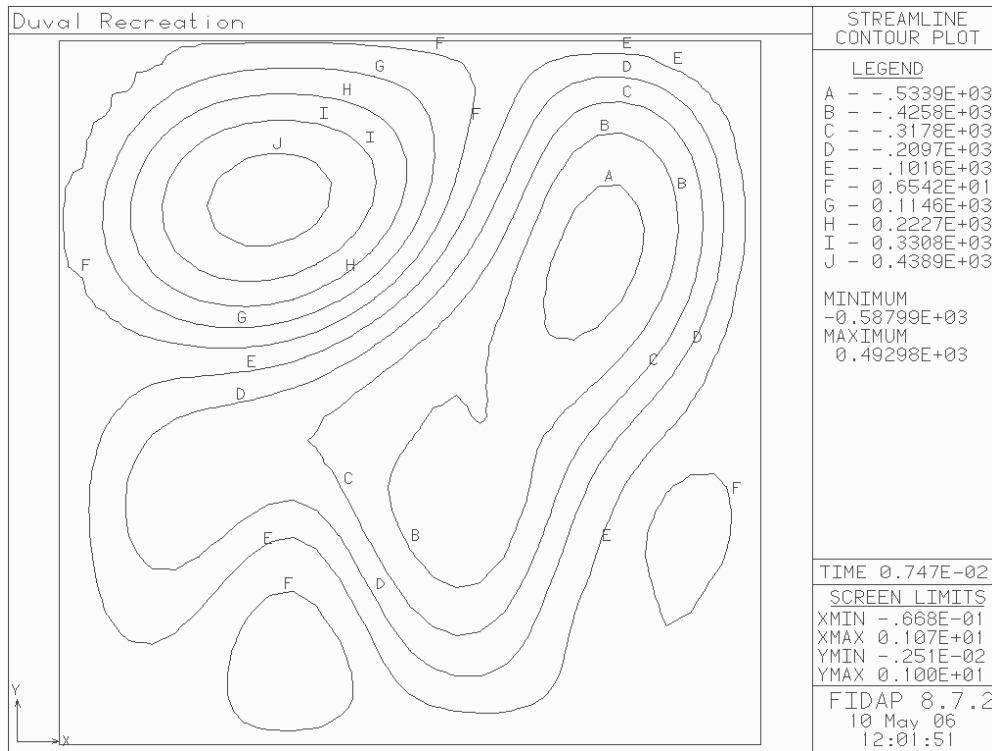

Figure 25: Flow structure for Case 4 at t* = 0.00356
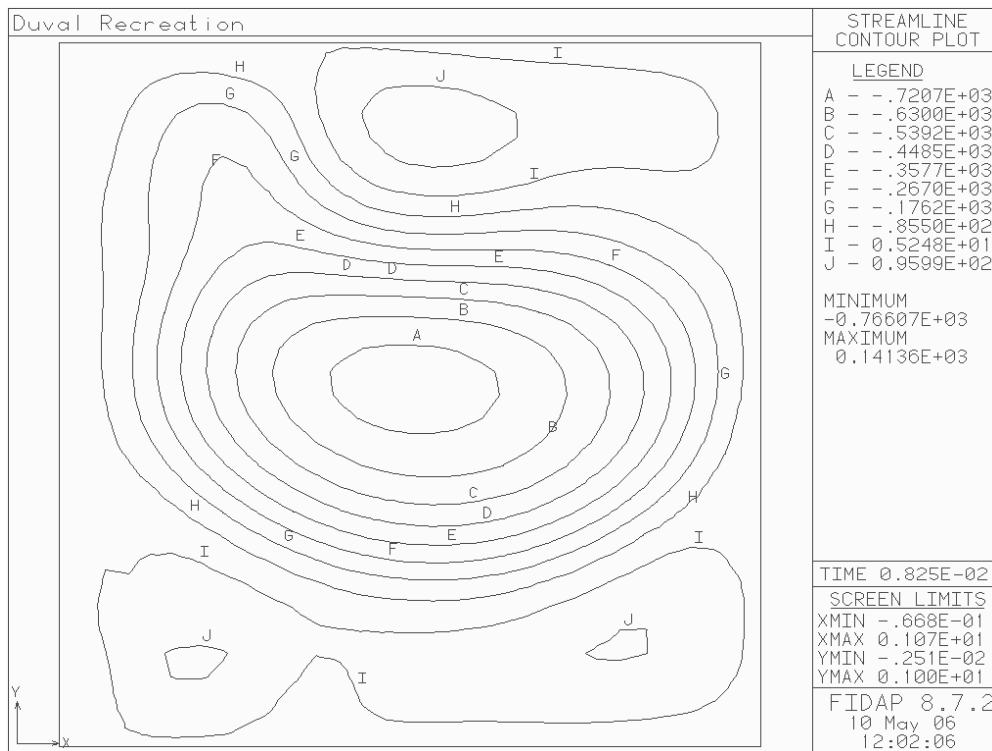
Figure 26: Flow structure for Case 4 at t* = 0.00747

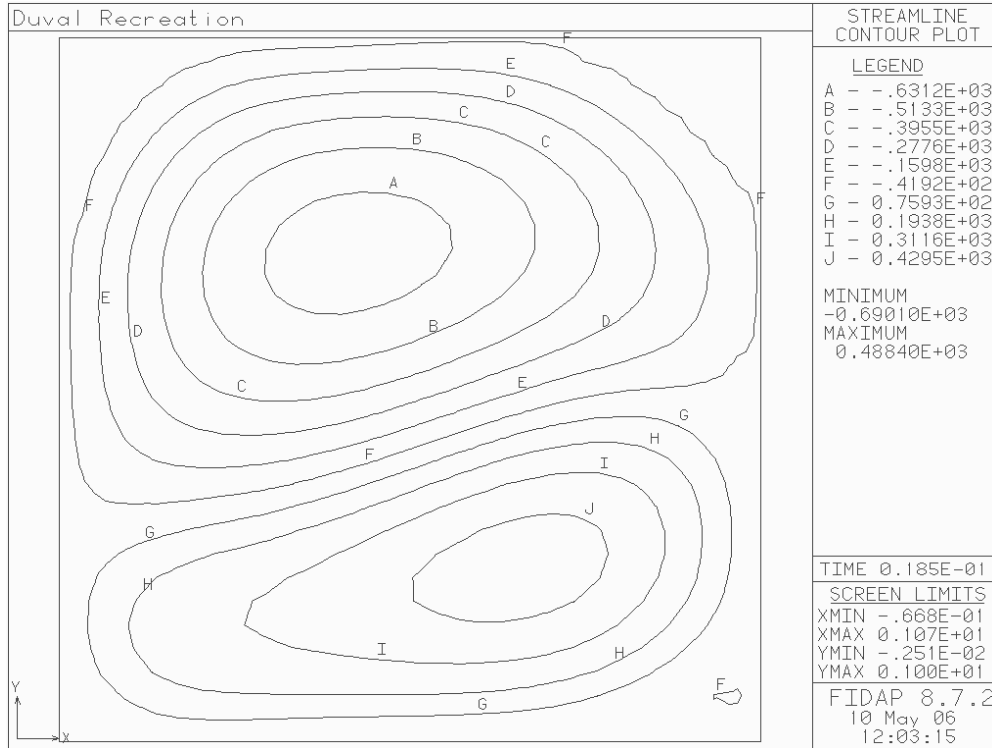Figure 27: Flow structure for Case 4 at t* = 0.00825

Figure 28: Flow structure for Case 4 at t* = 0.0185
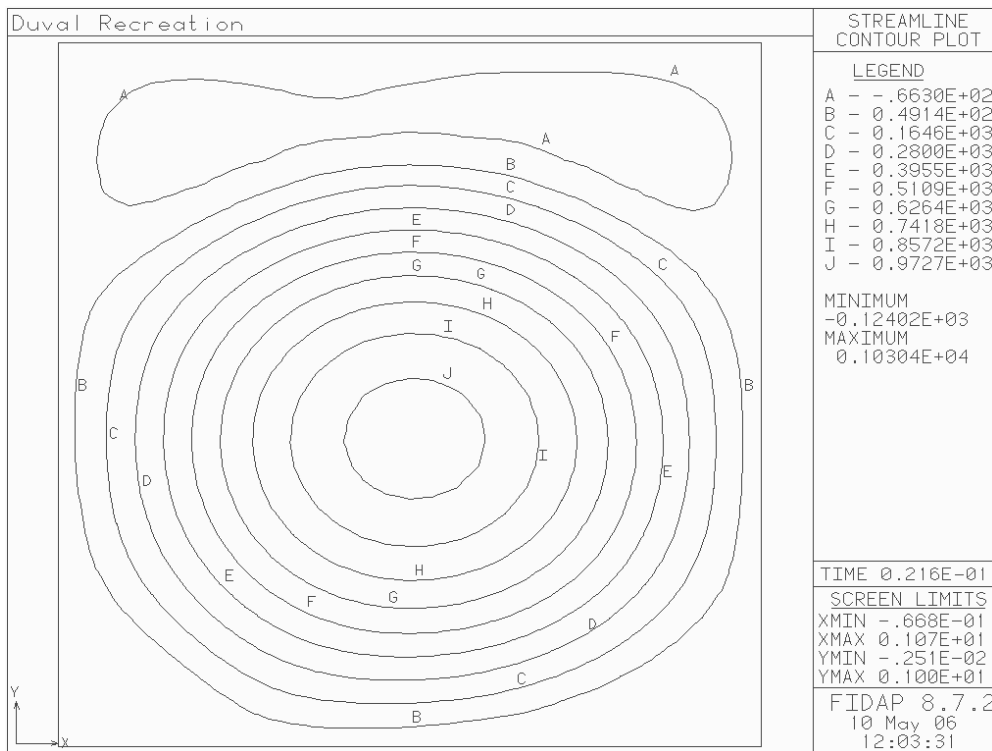

Figure 29: Flow structure for Case 4 at t* = 0.0216
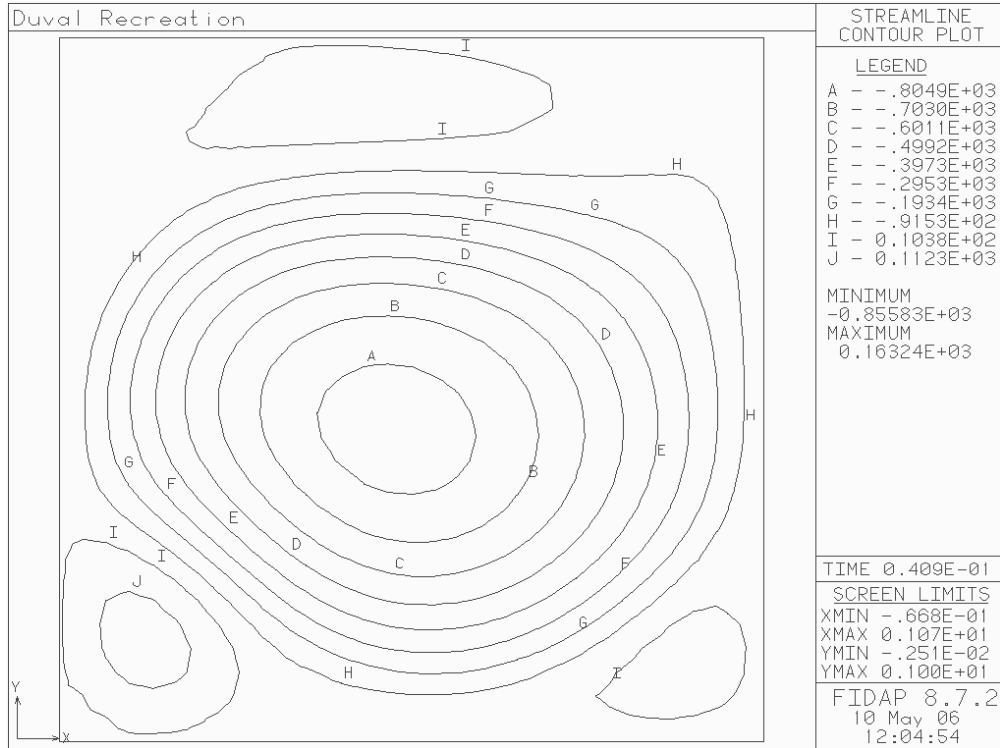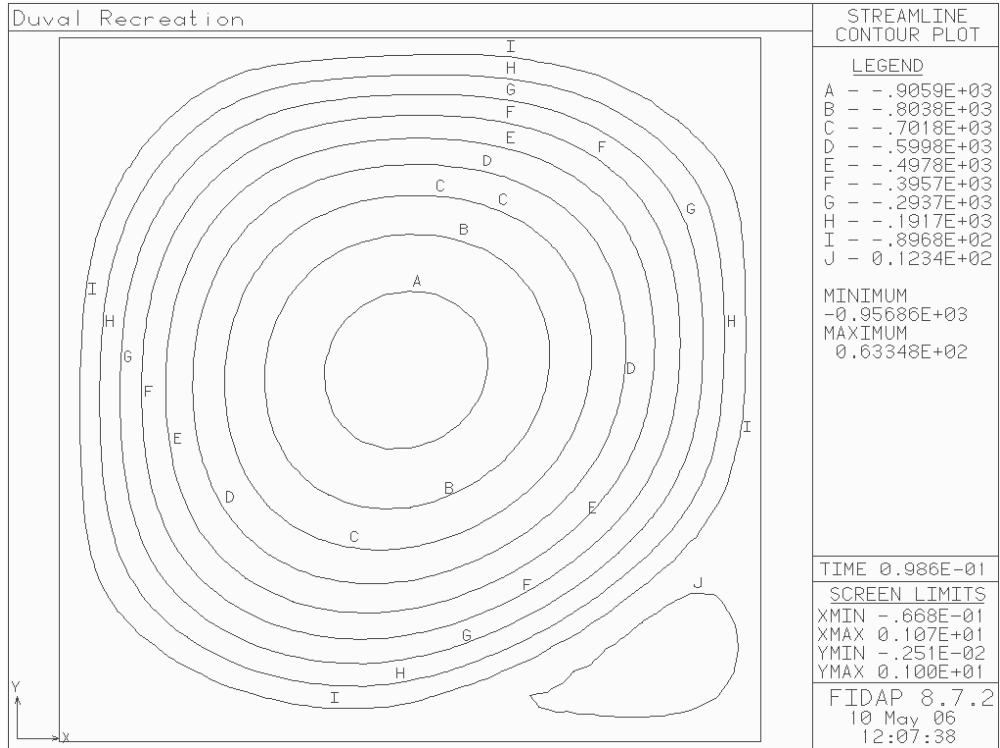
Figure 30: Flow structure for Case 4 at t* = 0.0409

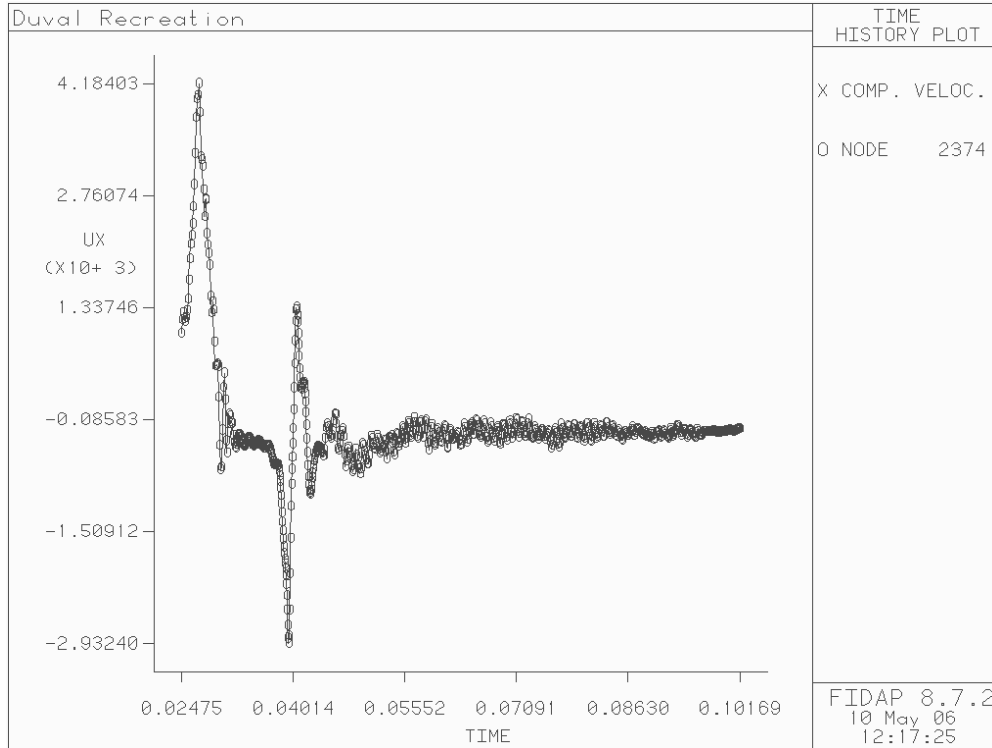Figure 31: Flow structure for Case 4 at t* = 0.0986

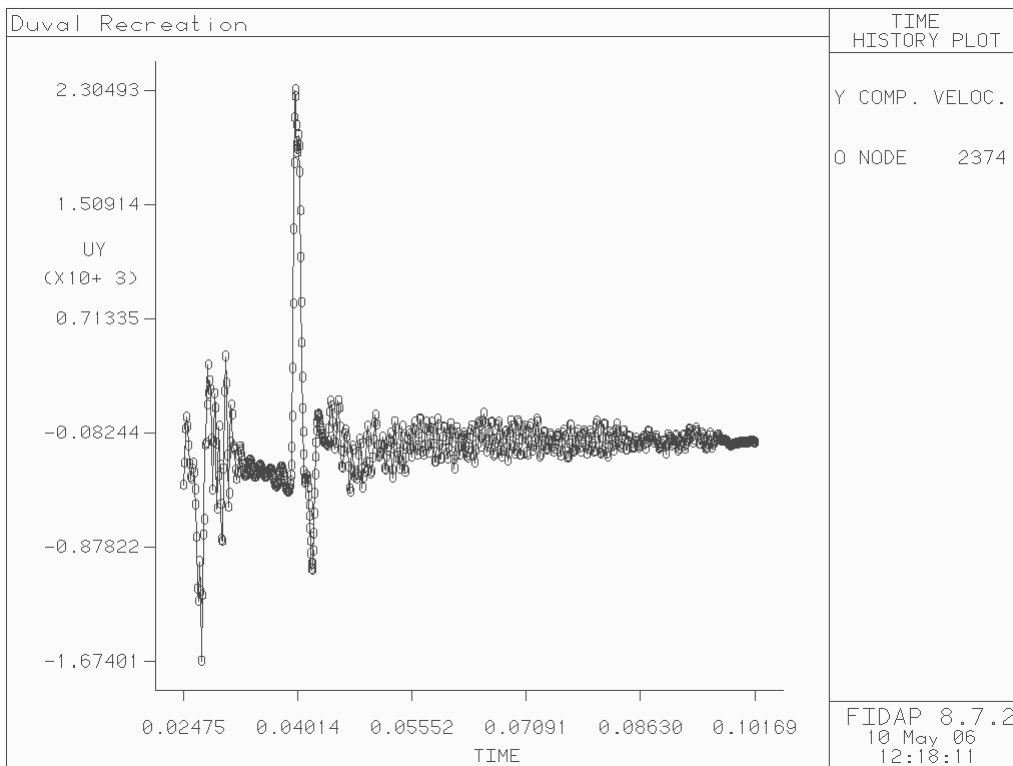Figure 32: Case 4 x-component velocity at a fixed point (0.5167, 0.5)

Figure 33: Case 4 y-component velocity at a fixed point (0.5167, 0.5)

Conclusions

The goal of this research was to create a computer model that would more accurately represent an actual PVT system than what has previously been done. This was done to get results that more closely represent what happens in an actual PVT system. This was accomplished by reducing the crystal size from the entire width of the simulated system to 20% of the width. The simulations were run using FIDAP software in order to compare results to previously solved cases. For the four cases that were run with the smaller crystal size and compared to the previous work done by Tebbe some similarities and some differences were found. Case 1 showed very similar characteristics to the previous research. Case 2 had one large difference when comparing the results. The previous research showed that the final flowfield structure was unicellular. This research shows that the flowfield transitions into a two-cell structure and stabilizes. Case 3 shows the largest amount of differences. Past research shows that again the final flowfield structure was unicellular whereas the current simulation depicts a two-cell final structure. Another large difference in this case is found in the time history velocity plots. The previous research showed that the velocity had continued oscillations over time. The current system shows that the velocity stabilizes at one value as it has done for Cases 1 and 2. The results of Case 4 show many similar traits to the previous research conducted. For this case the flowfield evolves into a unicellular structure and has some small oscillation over time. All together the new system looks as if it has moved the bifurcation points to slightly higher values. The ranges of Rayleigh numbers that were previously used to show these bifurcation regions may need to be adjusted to accurately represent the flowfield transition points. In order to find the new ranges of Rayleigh numbers more

research would need to be conducted to determine at what values for the Rayleigh number these transitions occur. This research may have an impact on the expected material quality and growth rates that had previously been determined.

References

[1] P.A. Tebbe, Finite Element Modeling of Asymmetric and Transient Flowfields during Physical Vapor Transport, Finite Elements in Analysis and Design 40 (2004) 1499-1519.

[2] W.M.B. Duval, Convection in the Physical Vapor Transport Process – I: Thermal, Journal of Chemical Vapor Deposition 2 (1994) 188-217.

Author's biography

Wade Luhman graduated from Minnesota State University Mankato with a Bachelor of Science in Mechanical Engineering in May of 2006. During his undergraduate studies Wade was active in the American Society of Mechanical Engineers (ASME) and had several internships. Wade performed in the Old Guard Poster and Oral Competitions at two different regional student conferences as part of his involvement with ASME. During the summer and fall semester of 2004 Wade worked for Hutchinson Technology Inc. as a co-op in the Advanced Process Development group. In the summer of 2005 he worked at Stanford University in California as part of an undergraduate research program through the National Nanotechnology Infrastructure Network. Currently Wade is working for Seagate Technology in Shakopee, Minnesota as an intern over the summer before starting graduate school in the fall. He will be attending the University of Minnesota in the Twin Cities to earn his Ph.D. in Materials Science.

Faculty mentor's biography

Patrick Tebbe is an Assistant Professor of Mechanical Engineering at Minnesota State University in Mankato. Dr. Tebbe received the B.S., M.S., and Ph.D. degrees in Mechanical Engineering as well as the M.S. in Nuclear Engineering from the University of Missouri – Columbia. He has active research in thermal-fluids area, numerical modeling of several materials processing applications, and pedagogical areas. He is currently a member of the American Society for Engineering Education, the American Society of Mechanical Engineers and the American Society of Heating, Refrigerating and Air-Conditioning Engineers.